



Cite this: RSC Adv., 2016, 6, 7999

Received 26th October 2015
 Accepted 5th January 2016

DOI: 10.1039/c5ra22402k
www.rsc.org/advances

Synthesis and properties of pteridine-2,4-dione-functionalised oligothiophenes†

Alan A. Wiles,^{‡,a} Brian Fitzpatrick,^{‡,a} Niall A. McDonald,^{‡,a} Mary Margaret Westwater,^a De-Liang Long,^a Bernd Ebenhoch,^b Vincent M. Rotello,^c Ifor D. W. Samuel^b and Graeme Cooke^{*a}

The synthesis of acceptor-functionalised oligothiophene derivatives (**t3**, **t6**, **t7**, **t8**) is described, where the pteridine-2,4-dione acceptor units are arranged symmetrically in derivatives **t6**–**t8**. The symmetrical arrangement of acceptor units stems from the ability to selectively brominate the conjugated thiophene moiety of building block **t3**. Upon increasing the conjugation by going from **t3** to **t8**, a significant increase in absorption toward the near-infrared region and a simultaneous narrowing of the HOMO/LUMO gap occurs, which may promote their future application as optoelectronic materials.

Introduction

Acceptor-functionalised short-chain linear oligothiophenes¹ have received considerable attention over recent years, and have been utilised as components in organic photovoltaic (OPV) cells, organic field effect transistors (OFETs), and organic light emitting diodes (OLEDs).² The juxtaposition of the thiophene donor (D) units with the acceptor (A) component affords conjugated D–A systems which typically promotes better charge carrier mobility and decreases the band gap.³ Therefore, the synthesis of new acceptor-appended short oligothiophenes are attractive targets for the development of promising new materials with a range of optoelectronic applications.

The pteridine-2,4-dione moiety occurs widely in biological systems, and in particular, is found in flavin-based redox cofactors.⁴ The fascinating redox properties of the latter have ensured that synthetic flavin derivatives have become important building blocks for systems with molecular device and optoelectronics applications.⁵ Here, we report a class of functionalised oligothiophene featuring pteridine-2,4-dione acceptor units which are constructed from building block **t3** (Scheme 1). An important feature of **t3** is that it is possible to selectively

brominate the α -position of one of the thiophene units thereby allowing the synthesis of oligothiophenes **t6**–**t8** with symmetrically appended acceptor units.

Results and discussion

Synthesis

The synthesis of the acceptor-functionalised oligothiophene derivatives are shown in Scheme 1. The synthesis of the key building block **t3** was achieved from compound **1**.⁶ *N*-Alkylation of **3** with iodoheptane was then undertaken to confer good solubility on **t3** and its resulting oligomers. The X-ray crystal structure of the **t3** clearly shows that one of the thiophene residues is almost coplanar to the pteridine core, whereas the other thiophene is non-planar and therefore non-conjugated to the core acceptor moiety (Fig. 1a). Bromination of **t3** furnished compound **4** in 71% yield following purification by column chromatography. ¹H NMR spectroscopy performed on compound **4** indicated that the bromination was selective, as evidence of other brominated species was not observed (see ESI†). X-ray crystallography confirmed that bromination occurs at the α -position of the more conjugated thiophene moiety (Fig. 1b). Compound **4** was then readily self-coupled (*via* the *in situ* preparation of its boronate ester) using a one-pot Suzuki–Miyaura reaction.⁷ Compound **4** could also be readily converted to oligothiophenes **t7** and **t8** using Stille methodology and the corresponding bis(tributylstannyl)thiophene.

Photophysical and electrochemical properties

UV-vis spectroscopy performed on compound **t3** indicated that the longest wavelength absorption band shows solvatochromism, which is consistent with an intramolecular charge-transfer (ICT) band (see ESI†). Increasing the oligothiophene chain length from **t3** to **t8** shifts the ICT absorption towards longer

^aGlasgow Centre for Physical Organic Chemistry (GCPOC), WestCHEM, School of Chemistry, University of Glasgow, Glasgow, G12 8QQ, UK. E-mail: Graeme.Cooke@glasgow.ac.uk

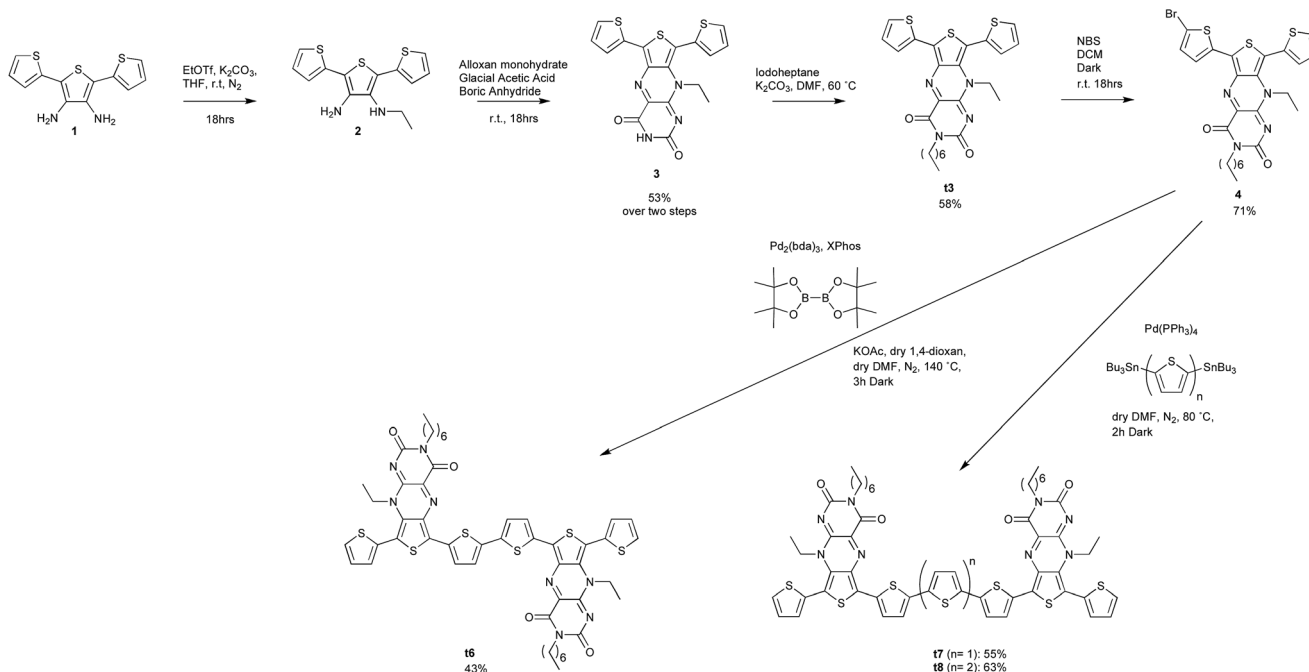
^bOrganic Semiconductor Centre, SUPA, School of Physics and Astronomy, University of St Andrews, North Haugh, St Andrews, Fife KY16 9SS, UK

^cDepartment of Chemistry, University of Massachusetts, Amherst, MA 01003, USA

† Electronic supplementary information (ESI) available: NMR spectra, cyclic voltammetry, fluorescence spectroscopy, X-ray crystallography. Open access data: <http://dx.doi.org/10.5525/GLA.RESEARCHDATA.249>. CCDC 1053866 and 1053867. For ESI and crystallographic data in CIF or other electronic format see DOI: 10.1039/c5ra22402k

‡ These authors contributed equally.





Scheme 1 Synthesis of t3, t6–t8.

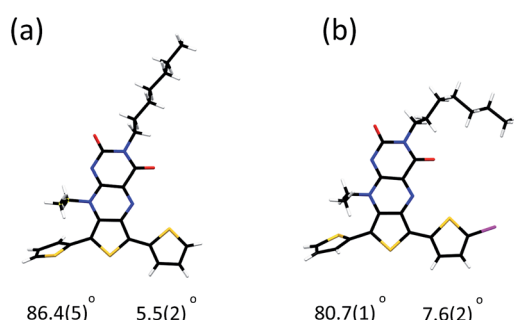
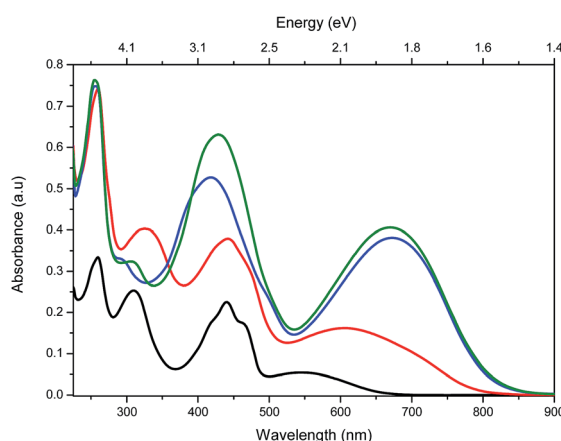


Fig. 1 X-ray crystal structures of derivatives (a) t3 and (b) 4. Colour scheme: C, black; H, grey; Br, pink; N, blue; O, red; S, yellow. Torsion angles with respect to central thiophene ring are provided.

Fig. 2 UV-vis absorption spectra of t3 (black), t6 (red), t7 (blue) and t8 (green) (1×10^{-5} M in DCM).

wavelength (547 nm for t3 to 673 nm for t8 in DCM) (Fig. 2). This chain length dependency in absorption properties suggests that the thiophene units are conjugated in the higher oligomers. The electrochemical properties of t3–t8 were determined using cyclic and square wave voltammetry (ESI† and Fig. 3). The electrochemical and optical properties are summarised in Table 1. The electrochemical data indicate that the oxidation potentials vary significantly whilst the reduction potentials remain fairly constant for the series. Accordingly, the calculated E_{fund} (ref. 8) on going from t3 to t8 significantly decreases, which mainly results from a lowering of the ionization potentials (IPs) due to a concomitant increase in conjugation within the thiophene backbone. However, the electron affinities (EAs) remain relatively unchanged, indicating that increasing the

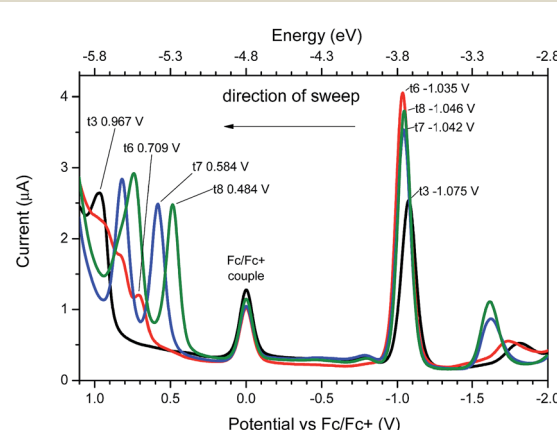
Fig. 3 Square wave voltammetry of t3 (black), t6 (red), t7 (blue) and t8 (green) (1×10^{-5} M in DCM).

Table 1 Summary of electrochemical and optical properties of **t3**, **t6**, **t8**, **t9**. E_{fund} (fundamental gap) = IP – EA. E_{opt} (optical gap) = $1240/\lambda_{\text{onset}}$

	Electrochemical properties					Optical properties		
	E_{ox} (V)	E_{red} (V)	IP (eV)	EA (eV)	E_{fund} (eV)	λ_{max} (nm)	λ_{onset} (nm)	E_{opt} (eV)
t3	0.97	–1.08	–5.8	–3.7	2.0	547	652	1.9
t6	0.71	–1.03	–5.5	–3.8	1.7	606	789	1.6
t7	0.58	–1.04	–5.4	–3.8	1.6	671	820	1.5
t8	0.48	–1.05	–5.3	–3.8	1.5	673	820	1.5

length of thiophene backbone has a limited influence on the acceptor properties of the pteridine units.

DFT calculations

DFT calculations were undertaken to probe the structure and electronic properties of **t3**–**t8**. The calculations for the oligomers are in accordance with the X-ray data for **t3**, and show that the outer thiophene units are out of conjugation with the acceptor core, whereas the conjugated thiophene units are essentially coplanar. The HOMOs of **t3**–**t8** are mainly located on the conjugated thiophene backbone whereas the LUMOs are largely localised over the pteridine acceptor cores and their conjugated thiophene units (Fig. 4 and ESI†). The calculated HOMO/LUMO energy trends are broadly in accordance with the electrochemically determined IP and EA energies (**t3** HOMO –5.8 eV, LUMO –3.1 eV; **t6** HOMO –5.4 eV, LUMO –3.3 eV; **t7** HOMO –5.2 eV, LUMO –3.3 eV; **t8** HOMO –5.2 eV, LUMO –3.2 eV), and further indicate that on going from **t3** to **t8** it is the HOMO/IP that is most affected ($\Delta\text{HOMO} = 0.6$ eV/ $\Delta\text{LUMO} = 0.2$ eV).

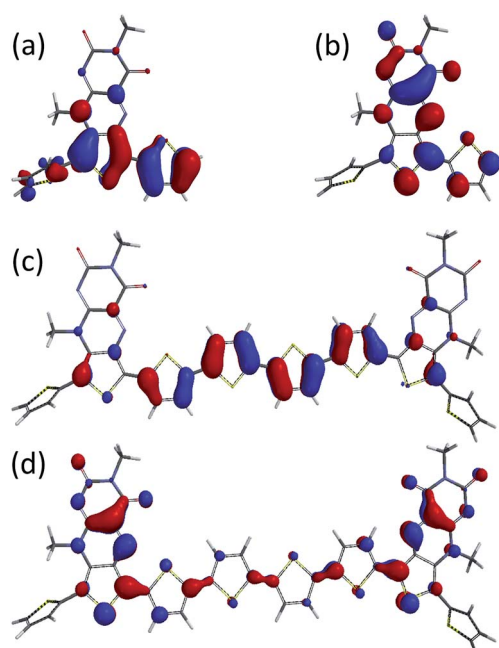


Fig. 4 DFT-calculated structures of **t3** and **t8** (alkyl groups replaced with methyl units) showing the HOMO ((a) and (c)) and LUMO ((b) and (d)) maps.

Spectroelectrochemistry

Spectroelectrochemical measurements were carried out on compounds **t3** (Fig. 5) and **t8** (Fig. 6). Application of increasing negative potential to the working electrode produced a profound change in their UV-vis spectra, and the applied potentials of which generally coincide with the onset of the reduction waves shown in Fig. 3. The UV-vis spectra of compound **t3** undergoes a significant change around –0.8 V with the peak at 439 nm collapsing and a new absorption at 471 nm forming. In accordance with spectroelectrochemical data recorded for related flavin derivatives, we attribute this spectral change due to the formation of pteridine radical anion species.⁹ As further negative potential is applied to the cell up to –1.2 V, the spectra pass through an isosbestic point at around 420 nm, whilst the absorption at 471 nm collapses and a shoulder at around 387 nm forms. This second feature is presumably due to the onset of the second reduced state (as indicated in the square wave voltammetry data). Interestingly, although the spectroelectrochemistry of **t8** is qualitatively similar to that of **t3** when a voltage of around –0.8 V is applied, in that a longer wavelength absorption at 445 nm and a shoulder around 480 nm form, however, a significantly longer wavelength absorption at 667 nm also forms for **t8**, which collapses with increasing negative potential. This new feature is likely a consequence of the addition of the second pteridine unit and the increased conjugation that occurs upon going from **t3** to **t8**, which significantly reduces the onset voltage required to generate the

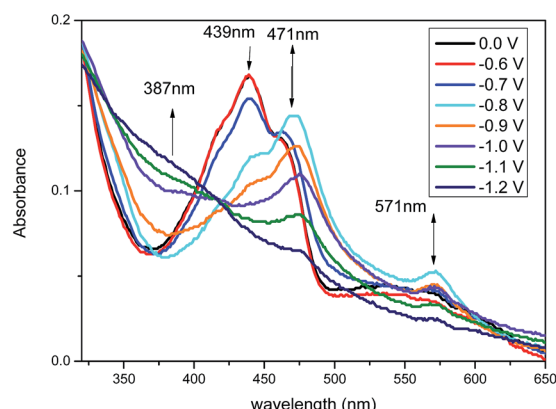


Fig. 5 Spectroelectrochemistry of **t3** recorded in DCM (1×10^{-4} M) using a platinum gauze working electrode, platinum wire counter electrode, silver wire pseudo-reference electrode and TBAPF₆ as electrolyte (0.1 M).



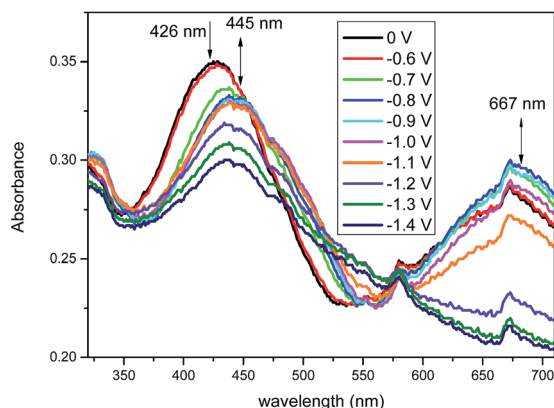


Fig. 6 Spectroelectrochemistry of **t8** recorded in DCM (1×10^{-4} M) using a platinum gauze working electrode, platinum wire counter electrode, silver wire pseudo-reference electrode and TBAPF₆ as electrolyte (0.1 M).

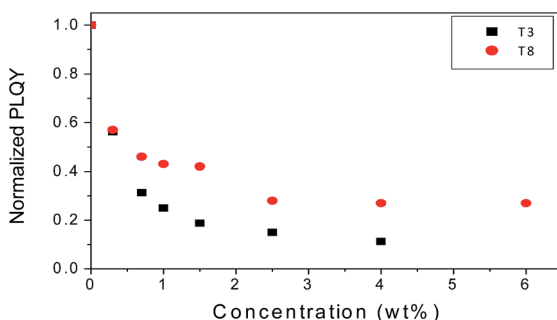


Fig. 7 The PLQY of P3HT as a function of increasing concentrations of **t3** and **t8**.

second reduced state. For both compounds the original spectra recover upon returning the applied potential to 0 V.

Fluorescence

The solution fluorescence of **t3** to **t8** were investigated, and experiments revealed that these materials were only weakly fluorescent, presumably a consequence of their donor-acceptor architecture. We next investigated the ability of **t3** and **t8** to quench the fluorescence of the electron rich polymer poly(3-hexylthiophene-2,5-diyl) (P3HT). Fig. 7 shows the photoluminescent quantum yield (PLQY) of thin film blends of these materials prepared from chlorobenzene solutions. Increasing the concentration of **t3** and **t8** to as little as 1% causes a significant (50%) quenching of the fluorescence of P3HT, thereby indicating efficient electron transfer from the donor polymer to acceptors **t3** and **t8**.¹⁰ At higher concentration of **t3** and **t8** (3%), no further quenching was observed indicating that significant aggregation of the **t3** and **t8** acceptor units may occur.

Experimental

All chemicals were purchased from commercial sources and used without further purification. (Sigma-Aldrich, TCI, Fisher,

Acros). TLC was performed using aluminium sheets coated with silica gel 60 F₂₅₄ (Merck). Dry solvents were obtained using Innovative Technology inc. Pure Solv 400-5-MD solvent purification system (activated alumina columns). IR spectra were recorded using a Perkin Elmer FT-IR instrument, ν_{max} is given in wavenumbers (cm⁻¹). Mass spectrometry was performed using a JEOL M STATION spectrometer. Melting points were measured using a SMP-10 Stuart Scientific melting point apparatus and are uncorrected. NMR spectroscopy was performed on either Bruker Avance 500 or a Bruker Avance 400 spectrometer. Spectra were processed using Mestrelab research iNMR© package (for MacOS X®). UV-vis and electrochemical data was processed using OriginLab©; Origin v. 8.5. Compound **1** was synthesised from 2,5-dibromothiophene.⁶

Synthesis

Compound 3. Compound **1** (0.8 g, 2.9 mmol) and K₂CO₃ (0.48 g, 3.5 mmol) were dissolved in dry THF (5 mL) under N₂ atmosphere. Ethyl trifluoromethanesulfonate (0.39 mL, 3.0 mmol) was then added slowly and the reaction was left to stir overnight under N₂. Water (100 mL) was added to the reaction mixture and the crude product was extracted into DCM (2 × 20 mL) and the organic extracts were dried over MgSO₄. The drying agent was then removed by filtration and the solvents were removed under vacuum to yield thiophene **2** as a dark brown solid. This was used without further purification and dissolved in glacial acetic acid (50 mL) with boric anhydride (0.47 g, 6.8 mmol) and alloxan monohydrate (0.56 g, 3.5 mmol). The reaction mixture was left to stir at room temperature overnight and the solvents were then removed under reduced pressure. The crude product was then purified by flash column chromatography (THF : hexane; 1 : 3) to yield **3** a red-greenish solid (0.63 g, 53%); mp > 300 °C; ν_{max} /cm⁻¹ (solid state) 3159 (N-H), 1673 (C=O); δ_{H} (500 MHz, CDCl₃) 1.22 (3H, t, *J* 7.0, CH₃), 4.43 (2H, q, *J* 7.0, CH₂), 7.17–7.20 (2H, m, CH), 7.34 (1H, dd, *J* 3.5, 1.2, CH), 7.60 (1H, dd, *J* 5.3, 1.2, CH), 7.63 (1H, dd, *J* 5.1, 1.0, CH), 7.83 (1H, dd, *J* 3.8, 1.0, CH), 8.48 (1H, s, NH); δ_{C} (125 MHz, CDCl₃) 12.7 (CH₃), 41.4 (CH₂), 106.1 (C), 107.4 (C), 127.4 (C), 127.5 (CH), 128.17 (CH), 129.0 (CH), 129.8 (CH), 130.6 (C), 131.6 (CH), 132.1 (C), 132.6 (CH), 133.9 (C), 135.1 (C), 142.3 (C=O), 150.3 (C=O); *m/z* (FAB⁺) 413.0202 [M + H]⁺ (C₁₈H₁₃N₄O₂S₃ requires 413.0201).

Compound t3. Iodoheptane (0.16 mL, 1.0 mmol) was added to a solution of compound **3** (0.15 g, 0.36 mmol) and potassium carbonate (0.19 g, 1.4 mmol) in acetone (20 mL). The reaction was stirred under reflux overnight. The solvent was then evaporated and the reaction quenched with water (20 mL). The crude product was extracted with chloroform (3 × 15 mL), washed with water (2 × 25 mL) and brine (2 × 25 mL). The combined organic extracts were then dried over MgSO₄, filtered and the solvent was removed under reduced pressure. The crude product was then purified by flash column chromatography (hexane/ethyl acetate; 3 : 1) to yield compound **t3** as a red solid (106 mg, 58%); mp 189–191 °C; ν_{max} /cm⁻¹ (solid state) 2951–2855, 1659, 1585, 1558, 1524, 1435; δ_{H} (500 MHz, CDCl₃) 0.87 (3H, t, *J* 6.8, CH₃), 1.18 (3H, t, *J* 7.0, CH₃), 1.25–1.42 (8H, m, CH₂), 1.72 (2H, dt, *J* 14.9, 7.5, CH₂), 4.06 (2H, t, *J* 7.5, CH₂), 4.37



(2H, q, *J* 7.0, CH₂), 7.14 (2H, ddd, *J* 5.1, 3.7, 1.1, CH), 7.31 (1H, dd, *J* 3.7, 1.1, CH), 7.56 (2H, ddd, *J* 5.1, 3.7, 1.1, CH), 7.78 (1H, dd, *J* 3.7, 1.1, CH); δ_{C} (125 MHz, CDCl₃) 12.9 (CH₃), 14.2 (CH₃), 22.7 (CH₂), 27.1 (CH₂), 28.0 (CH₂), 29.2 (CH₂), 31.9 (CH₂), 40.9 (CH₂), 42.3 (CH₂), 107.0 (C), 127.5 (CH), 127.6 (C), 128.1 (CH), 128.8 (CH), 129.7 (CH), 131.0 (C), 131.3 (CH), 132.4 (C), 132.6 (CH), 133.8 (C), 135.2 (C), 141.6 (C), 148.9 (C), 155.9 (C=O), 159.6 (C=O); *m/z* (FAB⁺) 511.1295 [M + H]⁺ (C₂₅H₂₇N₄O₂S₃ requires 511.1296).

Compound 4. Compound **t3** (170 mg, 0.32 mmol) was dissolved in DCM (10 mL) and the flask was covered with aluminium foil. *N*-Bromosuccinamide (64 mg, 0.36 mmol) was then added and the reaction mixture was left to stir overnight. The reaction was then quenched with water (100 mL) and the crude product extracted into DCM (3 × 50 mL). The combined organic extracts were then dried over MgSO₄, filtered and the solvent was removed under reduced pressure. The crude product was then purified by flash column chromatography (DCM 100%) to yield compound **4** as a green solid (158 mg, 81%); mp 242–244 °C; δ_{H} (500 MHz, CDCl₃) 0.88 (3H, t, *J* 6.9, CH₃), 1.18 (3H, t, *J* 7.0, CH₃), 1.26–1.43 (8H, m, CH₂), 1.69–1.75 (2H, m, CH₂), 4.06 (2H, t, *J* 7.7, CH₂), 4.37 (2H, q, *J* 7.0, CH₂), 7.10 (1H, d, *J* 4.0, CH), 7.15 (1H, dd, *J* 5.3, 3.5, CH), 7.31 (1H, dd, *J* 3.5, 1.2, CH), 7.43 (1H, d, *J* 4.0, CH), 7.57 (1H, dd, *J* 5.3, 1.2, CH); δ_{C} (125 MHz, CDCl₃) 12.9 (CH₃), 14.3 (CH₃), 22.8 (CH₂), 27.2 (CH₂), 28.0 (CH₂), 29.2 (CH₂), 31.9 (CH₂), 40.9 (CH₂), 42.4 (CH₂), 107.3 (C), 120.3 (CBr), 127.5 (C), 127.6 (CH), 128.2 (CH), 129.9 (CH), 130.6 (CH), 130.8 (C), 132.7 (CH), 133.8 (C), 133.9 (C), 135.3 (C), 140.4 (C), 149.0 (C) 155.8 (C=O), 159.5 (C=O); *m/z* (ES⁺) 611.0196 [M + Na]⁺ (C₂₅H₂₅⁷⁹BrN₄NaO₂S₃ requires 611.0215).

Compound t6. Compound **4** (120 mg, 0.2 mmol), tris(dibenzylideneacetone) dipalladium(0) (3.7 mg, 4.0 μ mol), bis(pinacolato)diboron (105 mg, 0.4 mmol), K₂OAc (40 mg, 0.4 mmol) and X-phos (40 mg, 8.0 μ mol) were added to a Schlenk tube, which was then evacuated and backfilled with N₂ gas three times. A mixture of dry 1,4-dioxane (15 mL) and dry DMF (5 mL) was added under N₂ and the tube was then sealed, protected from light and placed in an oil bath at 140 °C for 3 h. DCM (100 mL) was added and the organic layer was washed with water. The organic layer was dried over MgSO₄, filtered and the solvent evaporated under vacuum. The product was purified by column chromatography (100% DCM) to yield compound **t6** as a green solid (45 mg, 43%); mp 295–297 °C; $\nu_{\text{max}}/\text{cm}^{-1}$ (film) 2929, 2857, 1705, 1655, 1585, 1559, 1523, 1475; δ_{H} (500 MHz, CDCl₃) 0.86 (6H, t, *J* 6.9, CH₃), 1.16 (6H, t, *J* 6.9, CH₃), 1.41–1.21 (16H, m, CH₂), 1.60–1.67 (4H, m, CH₂), 4.03 (4H, t, *J* 8.0, CH₂), 4.35 (4H, q, *J* 6.9, CH₂), 7.13 (2H, dd, *J* 5.3, 3.6, CH), 7.27 (2H, d, *J* 4.0, CH), 7.28 (2H, dd, *J* 3.6, 1.2, CH), 7.55 (2H, dd, *J* 5.3, 1.2, CH), 7.64 (2H, d, *J* 4.0, CH); δ_{C} (125 MHz, CDCl₃) 12.9 (CH₃), 14.2 (CH₃), 22.8 (CH₂), 27.2 (CH₂), 28.0 (CH₂), 29.2 (CH₂), 31.9 (CH₂), 40.9 (CH₂), 42.4 (CH₂), 107.8 (C), 127.6 (CH), 127.6 (C), 129.0 (CH), 129.9 (CH), 130.8 (C), 132.6 (CH), 133.6 (CH), 134.1 (C), 135.5 (C), 135.9 (C), 140.3 (C), 140.9 (C=N), 148.9 (C=N), 155.8 (C=O), 159.5 (C=O); *m/z* (EI⁺) 1041.2123 [M + Na]⁺ (C₅₀H₅₀N₈O₄S₆Na requires 1041.2171).

Compound t7. Compound **4** (110 mg, 0.2 mmol), 2,5-bis(triptylstananyl)thiophene (55 μ L, 0.1 mmol) and tetrakis(triphenylphosphine)palladium(0) (6 mg, 5.0 μ mol) were added, under N₂ gas, to dry DMF (2 mL). The reaction was protected from light and stirred at 80 °C for 2 h. The reaction was terminated by diluting with DCM (75 mL) and then washed with water (3 × 75 mL), dried over MgSO₄ and filtered. The solvent was evaporated under vacuum and the product was purified by column chromatography (DCM 100%) to yield compound **t7** as a green solid (60 mg, 55%); mp > 300 °C; $\nu_{\text{max}}/\text{cm}^{-1}$ (film) 2929, 2857, 1704, 1653, 1584, 1557, 1510; δ_{H} (500 MHz, CDCl₃) 0.85 (6H, t, *J* 6.8, CH₃), 1.14 (6H, t, *J* 7.0, CH₃), 1.42–1.19 (16H, m, CH₂), 1.70–1.76 (4H, m, CH₂), 4.03 (4H, t, *J* 8.0, CH₂), 4.33 (4H, q, *J* 7.0, CH₂), 7.13 (2H, dd, *J* 5.0, 3.5, CH), 7.16 (2H, d, *J* 4.0, CH), 7.23 (2H, s, CH), 7.30 (2H, dd, *J* 3.4, 0.9, CH), 7.54 (2H, dd, *J* 5.3, 0.9, CH), 7.66 (2H, d, *J* 4.0, CH); δ_{C} (125 MHz, CDCl₃) 12.91 (CH₃), 14.25 (CH₃), 22.76 (CH₂), 27.18 (CH₂), 28.07 (CH₂), 29.23 (CH₂), 31.93 (CH₂), 40.87 (CH₂), 42.34 (CH₂), 106.88 (C), 124.85 (CH), 126.32 (CH), 127.57 (CH), 127.61 (C), 129.81 (CH), 129.89 (CH), 130.94 (C), 131.55 (C), 132.66 (CH), 133.32 (C), 135.49 (C), 136.81 (C), 140.99 (C), 142.77 (C=N), 148.97 (C=N), 155.87 (C=O), 159.60 (C=O); *m/z* (EI⁺) 1123.1996 [M + Na]⁺ (C₅₄H₅₂N₈O₄S₇Na requires 1123.2049).

Compound t8. Compound **4** (210 mg, 0.41 mmol), 5,5'-bis(triptylstananyl)-2,2'-bithiophene (0.12 mL, 0.2 mmol) and tetrakis(triphenylphosphine) palladium(0) (12 mg, 0.01 mmol) were added, under N₂ gas, to dry DMF (4 mL). The reaction was protected from light and stirred at 80 °C for 2 h. DCM (100 mL) was added and the organic layer was washed with distilled water (3 × 100 mL), dried over MgSO₄ and filtered. The solvent was evaporated under vacuum and the product purified by column chromatography (DCM 100%) to yield compound **t8** as a green solid (150 mg, 63%); mp > 300 °C; $\nu_{\text{max}}/\text{cm}^{-1}$ (film) 2923, 2853, 1704, 1651, 1582, 1556, 1530, 1509; δ_{H} (500 MHz, C₂D₂Cl₄) 0.91 (6H, t, *J* 6.8, CH₃), 1.19 (6H, t, *J* 7.0, CH₃), 1.46–1.24 (16H, m, CH₂), 1.67–1.71 (4H, m, CH₂), 4.00–4.03 (4H, m, CH₂), 4.34 (4H, q, *J* 6.8, CH₂), 7.17–7.19 (4H, m, CH), 7.22 (2H, d, *J* 3.9, CH), 7.30 (2H, d, *J* 4.0, CH), 7.34 (2H, dd, *J* 3.4, 1.0, CH), 7.61 (2H, dd, *J* 5.3, 1.0, CH), 7.73 (2H, d, *J* 4.0, CH); δ_{C} (125 MHz, C₂D₂Cl₄) 12.6 (CH₃), 14.1 (CH₃), 22.6 (CH₂), 26.9 (CH₂), 27.9 (CH₂), 29.0 (CH₂), 31.7 (CH₂), 40.8 (CH₂), 41.9 (CH₂), 106.9 (C), 124.7 (CH), 125.1 (CH), 126.1 (CH), 127.2 (C), 127.4 (CH), 129.7 (CH), 130.0 (CH), 130.3 (C), 131.0 (C), 132.5 (CH), 133.0 (C), 135.2 (C), 135.5 (C), 137.0 (C), 140.7 (C), 142.4 (C=N), 148.6 (C=N), 155.3 (C=O), 159.4 (C=O); *m/z* (EI⁺) 1205.1895 [M + Na]⁺ (C₅₈H₅₄N₈O₄S₈Na requires 1205.1931).

Spectroscopic and voltammetry measurements

UV-vis spectra were recorded on a Shimadzu UV-3600 spectrometer using a 10 mm path length quartz cuvette. Cyclic voltammetry and square wave voltammetry was recorded with a CH Instruments Inc. 440A potentiostat. The voltammograms were recorded in solutions of tetrabutylammonium hexafluorophosphate (TBAPF₆) in dry-DCM (0.1 M). Measurements were performed with degassed solutions under inert atmosphere, using a platinum working electrode, a silver wire



pseudo-reference electrode and a platinum wire counter electrode. The redox potentials were determined relative to the ferrocene/ferrocenium redox couple (4.8 eV), and IPs and EAs were estimated from these values.

UV-vis spectroelectrochemistry

Spectroelectrochemical measurements were carried out using the ALS Co. Ltd. SEC-C 0.5 mm spectroelectrochemical cell featuring a platinum gauze working electrode and silver wire pseudo-reference electrode and a platinum wire counter electrode. All experiments were carried out with 1×10^{-4} M solutions of the analyte in DCM with TBAPF₆ (0.1 M) as the supporting electrolyte. UV-vis spectra were recorded on a Shimadzu UV-3600 spectrometer, and potential was applied using a CH Instruments Inc. 440A potentiostat. A base line spectrum of the cell and electrolyte was subtracted from the recorded spectra and the spectra were re-zeroed.

Fluorescence quenching experiments

A solution of P3HT (from Rieke metals) was prepared by dissolving 20 mg mL⁻¹ in chlorobenzene. Solutions of **t3** and **t8** were prepared by dissolving 1 mg mL⁻¹ in chlorobenzene. Both solutions were mixed by appropriate volumes to yield the desired ratio of P3HT and **t3** and **t8** with the concentration given as the fraction of total mass. The solutions were then spin coated in a nitrogen filled glovebox at 1000 rpm. Quenching studies were performed by measuring the photoluminescence quantum yield with a Hamamatsu U6039-05 integrating sphere. At the excitation wavelength of 500 nm the total absorption was more than 60% and the emission was collected in a range from 650 to 900 nm. PLQY was determined by the instrument and is given by the number of photons emitted divided by the number of photons absorbed.

DFT calculations

Calculations were performed using a Spartan '14 (64-bit) software suite.¹¹ Molecular geometries were first optimised semi-empirically (AM1) and then re-optimised using DFT (B3LYP/6-31G*). Alkyl chains are substituted with methyl groups in order to diminish calculation time. The resulting structures were local minima, as none of the vibrational frequencies generated imaginary frequencies.

X-ray structure determination

Crystal data for **t3**: C₂₆H₂₈Cl₂N₄O₂S₃, $M_r = 595.60$, monoclinic system, space group P2₁/c, $a = 14.3594(3)$, $b = 22.1059(5)$, $c = 8.8264(2)$ Å, $\beta = 104.710(2)$, $V = 2709.91(10)$ Å³, $Z = 4$, $\rho_{\text{calcd}} = 1.460$ g cm⁻³; Mo_{Kα} radiation, $\lambda = 0.71073$ Å, $\mu = 0.504$ mm⁻¹, $T = 150$ K. 21011 data (5140 unique, $R_{\text{int}} = 0.0421$, $\theta < 25.7^\circ$) were collected on an Oxford Gemini A Ultra CCD diffractometer and were corrected for absorption (transmission 0.851–0.880). The structure was solved by direct methods and refined by full-matrix least-squares on F^2 to give $wR_2 = 0.1775$, $R_1 = 0.0576$, $S = 1.038$ for 362 parameters. Residual electron density extrema were 0.72 and -0.86 e Å⁻³.

Crystal data for **4**: C₂₅H₂₅BrN₄O₂S₃, $M_r = 589.58$, monoclinic system, space group P2₁/c, $a = 14.7336(8)$, $b = 18.2084(11)$, $c = 9.4057(6)$ Å, $\beta = 94.715(3)$, $V = 2514.8(3)$ Å³, $Z = 4$, $\rho_{\text{calcd}} = 1.557$ g cm⁻³; Mo_{Kα} radiation, $\lambda = 0.71073$ Å, $\mu = 1.915$ mm⁻¹, $T = 150$ K. 19655 data (4922 unique, $R_{\text{int}} = 0.0406$, $\theta < 26^\circ$) were collected on a Bruker Apex II Quasar CCD diffractometer and were corrected for absorption (transmission 0.846–0.945). The structure was solved by direct methods and refined by full-matrix least-squares on F^2 to give $wR_2 = 0.1037$, $R_1 = 0.0396$, $S = 1.051$ for 318 parameters. Residual electron density extrema were 0.96 and -0.56 e Å⁻³.

The crystallographic data for compound **t3** and **4** have been deposited with the Cambridge Crystallographic Data Centre with deposition number CCDC 1053866-1053867.

Conclusions

In conclusion, we report the synthesis of the symmetrically functionalised oligothiophene derivatives **t6**, **t7** and **t8** from building block **t3**. The increased conjugation that occurs on going from **t3** to **t8** results in a significant bathochromic shift in the maximum wavelength absorption and an E_{fund} as low as 1.5 eV. PLQY experiments reveal that these units have the propensity to act as efficient electron acceptors for the electron donor polymer P3HT.¹² It is anticipated that these, and related derivatives, will have interesting optoelectronics applications (e.g. photovoltaic properties).¹³ Our investigations will be reported in due course.

Acknowledgements

GC and IDWS thank the EPSRC for funding (EP/I00243X/1). VR thanks the NSF (CHE-1307021). IDWS also acknowledges support from a Royal Society Wolfson Research Merit Award.

Notes and references

- (a) L. Zhang, N. S. Colella, B. P. Cherniawski, S. C. B. Mannsfeld and A. L. Briseno, *ACS Appl. Mater. Interfaces*, 2014, **6**, 5327–5343; (b) A. Mishra, C.-Q. Ma and P. Bäuerle, *Chem. Rev.*, 2009, **109**, 1141–1276.
- For illustrative examples see: (a) J. J. Chen, T. L. Chen, B. Kim, D. A. Poulsen, J. L. Mynar and J. M. Fréchet, *ACS Appl. Mater. Interfaces*, 2010, **2**, 2679–2686; (b) Y. Liu, X. Wan, B. Yin, J. Zhou, G. Long, S. Yin and Y. Chen, *J. Mater. Chem.*, 2010, **20**, 2464–2468; (c) G. C. Welch, L. A. Perez, C. V. Hoven, Y. Zhang, X.-D. Dang, A. Sharenko, M. F. Toney, E. J. Kramer, T.-Q. Nguyen and G. C. Bazan, *J. Mater. Chem.*, 2011, **21**, 12700–12709; (d) Z. Li, G. He, X. Wan, Y. Liu, J. Zhou, G. Long, Y. Zuo, M. Zhang and Y. Chen, *Adv. Energy Mater.*, 2012, **2**, 74–77; (e) Y. Liu, X. Wan, F. Wang, J. Zhou, G. Long, J. Tian and Y. Chen, *Adv. Mater.*, 2011, **23**, 5387–5391; (f) J. Zhou, X. Wan, Y. Liu, G. Long, F. Wang, Z. Li, Y. Zuo, C. Li and Y. Chen, *J. Mater. Chem.*, 2011, **23**, 4666–4668; (g) Y. Liu, X. Wan, F. Wang, J. Zhou, G. Long, J. Tian, J. You, Y. Yang and Y. Chen, *Adv. Energy Mater.*, 2011, **1**, 771–775; (h)



G. He, Z. Li, X. Wan, Y. Liu, J. Zhou, G. Long, M. Zhang and Y. Chen, *J. Mater. Chem.*, 2012, **22**, 9173–9180; (i) G. He, Z. Li, X. Wan, J. Zhou, G. Long, S. Zhang, M. Zhang and Y. Chen, *J. Mater. Chem.*, 2013, **1**, 1801–1809; (j) G. Long, X. Wan, B. Kan, Y. Liu, G. He, Z. Li, Y. Zhang, Y. Zhang, Q. Zhang, M. Zhang and Y. Chen, *Adv. Energy Mater.*, 2013, **3**, 639–646; (k) X. Wan, Y. Liu, F. Wang, J. Zhou, G. Long and Y. Chen, *Org. Electron.*, 2013, **14**, 1562–1569; (l) T. S. van der Poll, J. A. Love, T.-Q. Nguyen and G. C. Bazan, *Adv. Mater.*, 2012, **24**, 3646–3649; (m) J. Zhou, Y. Zuo, X. Wan, G. Long, Q. Zhang, W. Ni, Y. Liu, Z. Li, G. He, C. Li, B. Kan, M. Li and Y. Chen, *J. Am. Chem. Soc.*, 2013, **135**, 8484–8487; (n) J. Zhou, X. Wan, Y. Liu, Y. Zuo, Z. Li, G. He, G. Long, W. Ni, C. Li, X. Su and Y. Chen, *J. Am. Chem. Soc.*, 2012, **134**, 16345–16351; (o) F. Baert, C. Cabanetos, A. Leliègue, E. Kirchner, O. Segut, O. Alévéque, M. Allain, G. Seo, S. Jung, D. Tondelier, B. Geffroy, J. Roncali, P. Leriche and P. Blanchard, *J. Mater. Chem. C*, 2015, **3**, 390–398; (p) P. J. Skabar, R. Berridge, I. M. Serebryakov, A. L. Kanibolotsky, L. Kanibolotskaya, S. Gordeyev, I. F. Perepichka, N. S. Sariciftci and C. Winder, *J. Mater. Chem.*, 2007, **17**, 1055–1062; (q) W. Zhang, S. C. Tse, J. Lu, Y. Tao and M. Shing Wong, *J. Mater. Chem.*, 2010, **20**, 2182–2189; (r) A. Riaño, P. Mayorga Burrezo, M. J. Mancheño, A. Timalsina, J. Smith, A. Facchetti, T. J. Marks, J. T. López Navarrete, J. L. Segura, J. Casado and R. Ponce Ortiz, *J. Mater. Chem. C*, 2014, **2**, 6376–6386; (s) T. Noda and Y. Shirota, *J. Am. Chem. Soc.*, 1998, **120**, 9714–9715.

3 E. Ahmed, G. Ren, F. S. Kim, E. C. Hollenbeck and S. A. Jenekhe, *Chem. Mater.*, 2011, **23**, 4563–4577.

4 S. O. Mansoorabadi, C. J. Thibodeaux and H.-W. Liu, *J. Org. Chem.*, 2007, **72**, 6329–6342.

5 (a) A. Niemz and V. M. Rotello, *Acc. Chem. Res.*, 1999, **32**, 44–52; (b) V. Nandwana, I. Samuel, G. Cooke and V. M. Rotello, *Acc. Chem. Res.*, 2013, **46**, 1000–1009.

6 X. Yangjun, J. Luo, X. Deng, X. Li, D. Li, X. Zhu, W. Yang and Y. Cao, *Macromol. Chem. Phys.*, 2006, **207**, 511–520.

7 F. Brouwer, J. Alma, H. Valkenier, T. P. Voortman, J. Hillebrand, R. C. Chiechi and J. C. Hummelen, *J. Mater. Chem.*, 2011, **21**, 1582–1592.

8 J.-L. Bredas, *Mater. Horiz.*, 2014, **1**, 17–19.

9 A. Niemz, J. Imbriglio and V. M. Rotello, *J. Am. Chem. Soc.*, 1997, **119**, 887–892.

10 P. E. Schwenn, K. Gui, A. M. Nardes, K. B. Krueger, K. H. Lee, K. Mutkins, H. Rubinstein-Dunlop, P. E. Shaw, N. Kopidakis, P. L. Burn and P. Meredith, *Adv. Energy Mater.*, 2011, **1**, 73–81.

11 Wavefunction Inc., 18401 Von Karman Ave., Suite 370, Irvine, CA 92612, USA.

12 A. F. Eftaiha, J.-P. Sun, I. G. Hill and G. C. Welch, *J. Mater. Chem. A*, 2014, **2**, 1201–1213.

13 L. Yuan, Y. Zhao, K. Lu, D. Deng, W. Yan and Z. Wei, *J. Mater. Chem. C*, 2014, **2**, 5842–5849.

